Frequency swept pulses for the enhanced resolution of ENDOR spectra detecting on higher spin transitions of Gd(III)

DOI:
10.1016/j.jmr.2023.107447

Document Version
Accepted author manuscript

Frequency swept pulses for the enhanced resolution of ENDOR spectra detecting on higher spin transitions of Gd(III)

Ciarán J. Rogers,[a] Alexey Bogdanov,[b†] Manas Seal,[b†] Matthew E. Thornton,[a] Xun-Cheng Su,[c] Louise S. Natrajan,[a] Daniella Goldfarb,[*b] and Alice M. Bowen[*a]

a) Department of Chemistry, Photon Science Institute and the National Research Facility for Electron Paramagnetic Resonance, School of Natural Sciences, The University of Manchester, Manchester, M13 9PL, UK.

b) Department of Chemical and Biological Physics, Weizmann Institute of Science, Rehovot, 7610001, Israel.

c) State Key Laboratory of Elemento-Organic Chemistry, Tianjin Key Laboratory of Biosensing and Molecular Recognition College of Chemistry, Nankai University, Tianjin 300071, China.

E-mail: alice.bowen@manchester.ac.uk ; daniella.goldfarb@weizmann.ac.il

[†] These authors contributed equally to this work.

Abstract

Half-Integer High Spin (HIHS) systems with zero-field splitting (ZFS) parameters below 1 GHz are generally dominated by the spin |−1/2>→|+1/2> central transition (CT). Accordingly, most pulsed Electron Paramagnetic Resonance (EPR) experiments are performed at this position for maximum sensitivity. However, in certain cases it can be desirable to detect higher spin transitions away from the CT in such systems. Here, we describe the use of frequency swept Wideband, Uniform Rate, Smooth Truncation (WURST) pulses for transferring spin population from the CT, and other transitions, of Gd(III) to the neighbouring higher spin transition |−3/2>→|−1/2> at Q- and W-band frequencies. Specifically, we demonstrate this approach to enhance the sensitivity of ^{1}H Mims Electron-Nuclear Double Resonance (ENDOR) measurements on two model Gd(III) aryl substituted 1,4,7,10-tetraazacyclododecane-1,4,7-triacetic acid (DO3A) complexes, focusing on transitions other than the CT. We show that an

enhancement factor greater than 2 is obtained for both complexes at Q- and W-band frequencies by the application of two polarising pulses prior to the ENDOR sequence. This is in agreement with simulations of the spin dynamics of the system during WURST pulse excitation. The technique demonstrated here should allow more sensitive experiments to be measured away from the CT at higher operating temperatures, and be combined with any relevant pulse sequence.

Introduction

Electron-Nuclear Double Resonance (ENDOR) spectroscopy is a widely applied pulsed Electron Paramagnetic Resonance (EPR) technique to determine the electronic and geometric properties of paramagnetic centres coupled to magnetically active nuclei.[1,2] In particular, ^{1}H ENDOR spectroscopy has found a wide range of uses in areas ranging from atomistic structure determination in protein samples[3–6] to the investigation of the electronic properties of superconducting quantum dots.[7,8] ^{1}H ENDOR can provide, in favourable conditions, electron-proton distances and proton orientational arrangement, and is therefore of high importance in revealing the structure-function relationships of the active sites of many metalloenzymes and biomimetic models thereof.[9–12]

Gadolinium(III) complexes are routinely used as spin labels at Q- and W-band frequencies for long-range distance determination by pulsed dipolar EPR, namely Double Electron-Electron Resonance (DEER), primarily due to in-cell stability[13–15] and the absence of orientation selection.[16,17] More recently, Gd(III) labels have been employed for short-range ENDOR based distance measurements in model systems and proteins.[18,19] Gd(III), a half-integer high spin (HIHS) (S = 7/2) ion, is characterised by a relatively small zero-field splitting (ZFS) and therefore its low temperature (frozen solution) spectrum is dominated by a narrow $|-1/2\rangle \rightarrow |+1/2\rangle$ central transition (CT) at Q- and W-band at temperatures above 5 and 10 K respectively. The higher spin transitions usually appear as a broad featureless background of relatively low intensity onto which the sharp CT is superimposed. ENDOR measurements are usually carried out at a magnetic field corresponding to the maximum intensity of the EPR spectrum, namely the CT. However, there are instances where ENDOR measurements targeting the higher spin transitions of HIHS systems are of interest as they can facilitate the disentanglement of overlapping spectral signals, and resolve coupling to nuclei with $|m_I| > \pm 1/2$ (*e.g.* ^{17}O) allowing the nuclear quadrupole interaction to be determined.[20] Specifically, assignment of ENDOR transitions to higher spin manifolds of Gd(III) can give direct readings

of the anisotropic hyperfine constant, $T_{\perp}$, allowing the Gd(III) interaction with outer sphere water molecules in MRI contrast agents to be determined.[21] Furthermore, the sign of the hyperfine interaction can be readily determined by selective excitation of specific EPR transitions away from the CT in HIHS systems.[22,23] Alternatively, if the $|m_S| = \pm 1/2$ contribution to the Gd(III) ENDOR spectrum is of sole interest, a measurement away from the CT can be subtracted from a measurement targeting the CT to give a spectrum solely dependent on the coupling of the nuclear transitions within the $|m_S| = \pm 1/2$ manifold.[24] However, unless such measurements targeting the higher spin manifolds of Gd(III) are carried out at high fields and/or very low temperatures that increase the populations of these transitions, they can suffer from low signal-to-noise ratios (SNR) and long measurement times. The small spectral width of the employed detection pulses further limit sensitivity of ENDOR measurements targeting higher spin manifolds, and are often orders of magnitude lower than the width of the transitions.

The commercial availability of fast Arbitrary Waveform Generators (AWGs) has afforded pulse shaping capabilities previously unachievable on the timescales of an EPR experiment.[25] This has allowed for the development of pulse shaping techniques that permit polarisation transfer between EPR transitions for signal enhancement in HIHS systems. These techniques were originally developed for transferring polarisation from satellite transitions to the CT in quadrupolar NMR.[26,27] When applied to EPR, polarisation transfer was shown to give a signal enhancement of 85% in DEER distance measurements measured on a Gd(III)-Gd(III) ruler with a ZFS parameter < 1 GHz.[28] To achieve this, adiabatic frequency swept pulses were designed to pre-polarise the system by altering the equilibrium populations of the EPR transitions before application of the DEER sequence. Prior to this, it had been reported in a Mn(II) doped in MgO ($S = 5/2$) system that a low powered microwave pulse over the $|{-}3/2\rangle \rightarrow |{-}1/2\rangle$ transition, in combination with a rapid magnetic field sweep, transfers spin population to the CT of Mn(II) resulting in a polarisation enhanced spectrum, with subsequent polarised ENDOR measurements showing a maximum signal enhancement of 50%.[29]

In this work, we present the generation of adiabatic and bandwidth tuned frequency swept and Wideband, Uniform Rate, Smooth Truncation (WURST) amplitude modulated pulses at Q-band (33.93 GHz) for enhanced echo sensitivity when detecting on the $|{-}3/2\rangle \rightarrow |{-}1/2\rangle$ EPR transition of a model Gd(III) aryl substituted 1,4,7,10-tetraazacyclododecane-1,4,7-triacetic acid (DO3A) complex (**1**) (Figure 1) at 4.5 K. Similar measurements were also carried out at W-band (94.9 GHz) on a Gd(III) BrPsPy-DO3A complex (**2**) (Figure 1) at 11.5 K. The enhancement achieved from transferring spin

polarisation from the CT to the |−3/2>→|−1/2> transition by means of a pre-polarising shaped pulse was demonstrated in Hahn Echo-Detected Field Swept (EDFS), stimulated EDFS, and ^{1}H Mims ENDOR sequences, with consistent enhancement factors across different experimental timescales. Further, the controlled generation of polarisation using two consecutive frequency swept and WURST amplitude modulated pulses on either side of the |−3/2>→|−1/2> transition transferred polarisation from both the CT and a portion of the |−5/2>→|−3/2> and |−7/2>→|−5/2> transitions, resulting in an increased enhancement of the detection spin echo on the |−3/2>→|−1/2> transition.

Experimental

Sample preparation

Chemical structures of the studied Gd(III) complexes are presented in Figure 1. Complex (**1**) was synthesised according to the procedure described in the SI (Section S1), while complex (**2**) was prepared as described previously.[30] For Q-band measurements, a 200 µM solution of (**1**) in D_2O/d_8-glycerol (20% v/v) was placed in a 1.8 mm quartz tube (outer diameter, O.D.). For W-band measurements, a 200 µM solution of (**2**) in D_2O/d_8-glycerol (20% v/v), was placed in a 0.6 mm (inner diameter, I.D.) quartz capillary.

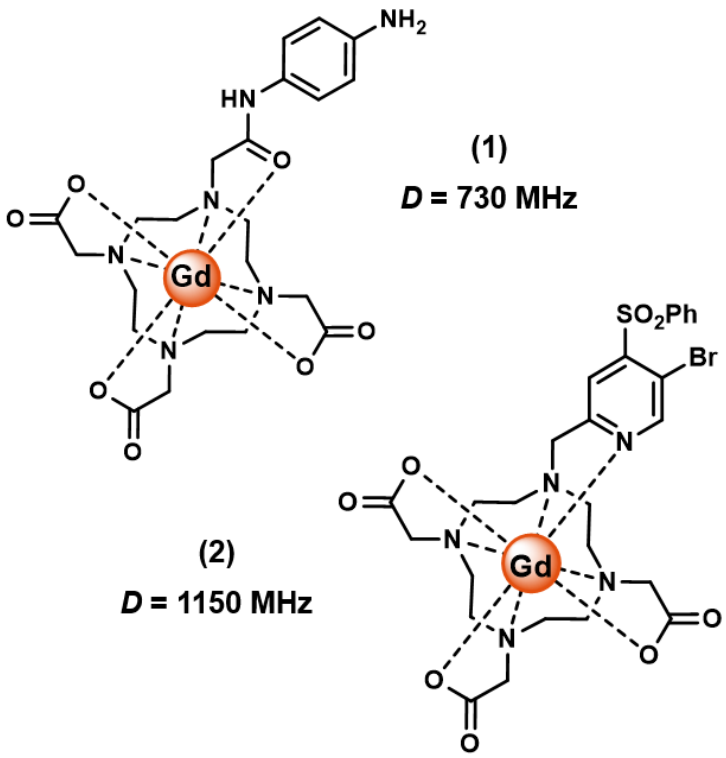

Figure 1: *Model Gd(III) complexes investigated for polarisation transfer experiments at Q-band (**1**) and W-band (**2**), noting the ZFS parameter, D, of each complex.*

Spectroscopic measurements

All EPR measurements at Q-band were performed at 4.5 K on a Bruker ELEXSYS E580 spectrometer equipped with a fully over-coupled Bruker EN 5107D2 resonator, a Bruker SpinJet AWG, and a liquid helium flow cryostat (CF935, Oxford Instruments), using AWG pulses as discussed in detail below. All pulses were amplified via a pulsed travelling wave tube (TWT) amplifier (150 W). Initially a resonator profile was obtained from transient nutation experiments at variable frequency detecting on the Gd(III) signal maximum of complex (**1**) (1218.7 mT at 33.93 GHz). The length of the first pulse (*p*) was incremented (*p–T–π/2–τ–π–τ–echo*) in 2 ns time steps over a period of 200 ns and T = 5 μs to ensure that any coherences generated by the first pulse had decayed before the detection sequence (Figure S.3.2). The maximum nutation frequency υ_1 (and corresponding B_1) was found to occur at 33.93 GHz and at this frequency rectangular microwave pulses of $\pi/2$ = 8 ns and π = 16 ns, generated through the AWG, were optimally tuned with an AWG amplitude of 4%, corresponding to a υ_1 of 31.25 MHz. The maximum achievable υ_1 at this frequency, at 100% AWG amplitude, was 250 MHz, as measured from the resonator profile. Reference Hahn EDFS (*π/2–τ–π–τ–echo*) and stimulated EDFS (*π/2–τ–π/2–t– π/2–τ–echo*) with no pre-polarising pulses were recorded using these pulses, with τ = 400 ns, t = 13 μs and a repetition time of 7.5 ms. Radiofrequency (RF) π-pulses were amplified using a 2 kW RF amplifier. The RF π-pulse was tuned by a transient RF nutation experiment on the proton line at 51.6 MHz, where the length of the RF π-pulse was incremented in 100 ns steps (*π/2–τ–π/2–t_{rf}–T–π/2–τ–echo*) where t_{rf} + T = 20 μs (Figure S.3.2). ^{1}H Mims ENDOR experiments in the absence of pre-polarisation were recorded for reference using the sequence *π/2–τ– π/2–t_{rf}–π/2–τ–echo* where t_{rf} = 13 μs, and the length of the RF π-pulse = 11 μs. For the polarisation transfer experiments, two polarisation pulses were used which were swept +300 to +100 MHz (pulse A), or –300 to –100 MHz (pulse B), relative to the detection frequency (33.93 GHz). These were compensated to the cavity profile as described in the results section. Final optimisation was carried out by performing a nutation experiment of the amplitude of the off-resonance shaped pulse (π_{AWG}*–T–π/2–τ–π–τ–echo*), with T = 2 μs, at a field position that placed this pulse resonant with the CT; 1225.8 mT for pulse A and 1211.6 mT for pulse B (further details available in SI). The amplitude chosen for the experiment corresponded to the maximum in the detected echo. The polarisation enhancement was confirmed by measuring Hahn EDFS and stimulated EDFS with either one or both of the shaped pulses using the sequences *P–T–π/2–τ–π–τ–echo* and *P–T–π/2–τ–π/2–t–π/2–τ–echo*, where *P*, the polarisation sequence can be either shaped pulse A ($\pi_{AWG,A}$), shaped pulse B ($\pi_{AWG,}$

$_{B}$), or both separated by a 200 ns gap ($\pi_{AWG,\,A}$–*200 ns*–$\pi_{AWG,\,B}$) and T = 2 μs to ensure that any on-resonance coherences generated by the shaped pulses had decayed. Full details of the polarisation pulses (pulse A and pulse B) are given below and their parameters given in Table S.3.2 (Supporting Information). The Mims ENDOR sequence was preceded by either one or two shaped polarisation pulses with a delay of T = 2 μs between the end of the final polarisation pulse and the beginning of the ENDOR sequence. In the case of two polarisation pulses, a delay of t = 200 ns was placed between them ($\pi_{AWG,\,A}$–t–$\pi_{AWG,\,B}$–T–$\pi/2$–τ–$\pi/2$–t_{rf}–$\pi/2$–τ–*echo*). RF frequencies were sampled using both stochastic and non-stochastic (linearly swept) RF π-pulses within the spectral region of interest. 50 scans were collected for ENDOR measurements in all cases. Mims ENDOR datasets were phased to minimise the imaginary component before plotting and were collected with 1 shot per point and a step size of 10 KHz.

W-band measurements were carried out on a home-built spectrometer at 11.5 K.[31] Echo decays and EDFS measurements were acquired with a two-step phase cycle and the microwave pulses were set to $\pi/2$ = 15 ns and π = 30 ns, with τ = 500 ns, and a repetition time of 1 ms. The magnetic field was chosen either to observe at the CT (3418 mT at 94.9 GHz) or where the contribution of the |─3/2>→|─1/2> transition (3412 mT at 94.9 GHz) is dominating. The bandwidth of the ENDOR cavity (Figure S.3.3, Supporting Information) was measured using a nitroxide solution at 50 K and a nutation sequence as described above, and was further scaled to the Gd(III) ν_1 value according to a nutation experiment carried out on the CT at the centre of the resonator profile. ^{1}H Mims ENDOR experiments were recorded using the sequence $\pi/2$–τ–$\pi/2$–t_{rf}–$\pi/2$–τ–*echo*. Additional delays of 200 ns before and 4 μs after the RF π-pulse were added in order to avoid artefacts from ring-down effects. RF π-pulses were amplified using a RF amplifier (TOMCO BT02000-GammaS RF amplifier, peak envelope power 2kW). The RF π-pulse length was 28 μs and was tuned by a transient RF nutation experiment on the proton line at 144.5 MHz (Figure S.3.3). RFs were sampled stochastically within the spectral region of interest. For the polarised experiments, two WURST pulses (pulse C: 94.5 GHz to 94.84 GHz and pulse D: 94.96 GHz to 95.4 GHz), relative to the observation frequency of 94.9 GHz, were applied followed by a time delay of T = 2 μs between the end of the final polarisation pulse and the beginning of the corresponding pulse sequence. The shaped pulses were not corrected for the cavity profile. The detailed parameters of the polarisation pulses are given in Table S.3.3, Supporting Information. 10 scans were collected for ENDOR measurements at the CT whereas 40 scans were collected at the |─3/2>→|─1/2> transition.

Mims ENDOR datasets were collected with 1 shot per point, two-step phase cycling, and a step size of 25 KHz.

Spectral simulations, the generation of bandwidth compensated shaped pulse files, spectral analysis and plotting of data was performed in MATLAB R2020a, using *EasySpin* 5.2.30 simulation software. All files are available in the repository detailed in the SI.

Results and discussion

Q-band

In order to optimise polarisation transfer using shaped frequency swept pulses, it was necessary to determine the resonator cavity profile so as to generate polarising pulses that compensate for the available bandwidth and non-linear power profile of the resonator at different frequency offsets. This was not implemented in the W-band measurements, where the cavity profile is significantly flatter and more uniform (Figure S.3.3). In each pre-polarised experiment targeting the CT, the detection pulses set to the |−3/2>→|−1/2> transition were placed at the centre of the resonator profile (33.93 GHz) and the shaped frequency swept pulses offset between ±100 to ±300 MHz. The adiabaticity factor of the linear frequency swept WURST amplitude modulated pulse, at its minimum, is defined as:

$$Q_{min} = \frac{\omega_1^2 t_p}{\Delta\omega} \quad (1)$$

where ω_1 is calculated from the measured υ_1 nutation frequency (in MHz) for the central transition of the Gd(III) spin system according to $\omega_1 = 2\pi\upsilon_1/\sqrt{S(S+1) - m_s(m_s+1)}$, t_p is the pulse length, and $\Delta\omega$ is the given spectral bandwidth.[25] For $Q_{min} \geq 5$, quantitative inversion is achieved for a spin-1/2 system, however lower values of Q_{min} can be used in high spin systems as the transition moment on individual transitions is larger.[28] It should also be noted that if the value of υ_1 at a specific offset falls below that required for adiabatic inversion this can be partially compensated by considering the resonator profile in the pulse design (further details available in SI, Figure S.3.4). All shaped polarisation pulses satisfying the adiabatic condition were generated using the *EasySpin*[32] pulse function. The polarisation pulses used were linear frequency swept pulses with a WURST amplitude envelope of the form:

$$A_{WURST} = 1 - \left|\sin\frac{\pi t}{t_p}\right|^{nwurst}$$

where *nwurst* = 5, t_p = 100 ns, t = [-t_p/2, +t_p/2]. The final shaped pulses are frequency swept from [+300, +100] (pulse A) or [−300, −100] MHz (pulse B) relative to the detection frequency [0 MHz], and are compensated for the resonator bandwidth within the *EasySpin* pulse function (Figure S.3.5).

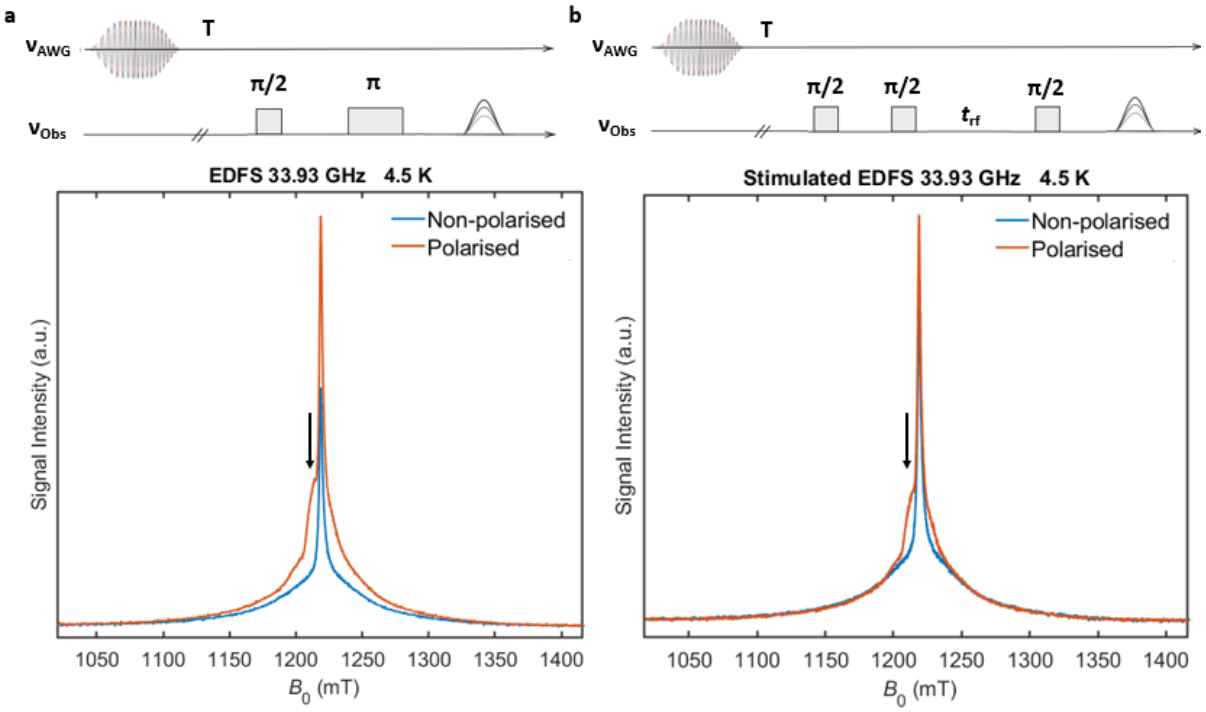

Figure 2: *Experimental Hahn EDFS (a) and stimulated EDFS (b) spectra of complex (**1**), and corresponding pre-polarised pulse sequences (pulse B), at 4.5 K (33.93 GHz) with no pre-polarising pulse (blue) or one optimised pre-polarising pulse (pulse B, orange). The conditions for optimal pre-polarisation were determined by an amplitude sweep of echo intensity at 1211.6 mT (arrows) and 33.93 GHz (Figure S.3.6).*

Initial measurements investigated the enhancement observed in a simple Hahn Echo detection sequence optimised for (**1**) in deuterated solvent (τ = 400 ns) (Figure 2a). At a field position of 1211.6 mT (33.93 GHz), where the detection pulses target the |−3/2>→|−1/2> transition (arrows, Figure 2), an enhancement factor of ca. 2 was obtained. A stimulated EDFS spectrum with time delays relevant to a Mims ENDOR experiment with a RF π-pulse length of 11 μs (i.e. a time delay of 13 μs between the second and third π/2 pulses) was recorded and showed significant retention of polarisation, with an enhancement of 1.72 at the same field position (Figure 2b). It should be noted that in the field swept spectra the polarisation pulse applied is only fully on-resonance with the CT at a field position of 1211.6 mT. At other field positions this pulse is resonant with other parts of the spectrum and other polarisation pathways

may be occurring. This explains the reduction in polarisation, observed further away from the CT in these spectra.

Simulations of the temporal evolution of spin polarisation on the detected transition during the application of the polarising pulse were performed with home-written Matlab scripts using the *Spidyan*[33] library, as described previously,[28] and used elsewhere to simulate pulse EPR experiments with arbitrary waveform generated excitation pulses.[34] For fitted ZFS parameters of complex (**1**) of D = 730 MHz and E = 140 MHz, a weighted Gaussian distribution of D values with a FWHM of 830 MHz accounting for the strain in D, and powder averaging over different orientations of the ZFS tensor with respect to the external magnetic field (full details in SI), the simulated evolution of polarisation in the rotating frame agreed well with the experimental enhancement seen in the initial field swept measurements, demonstrating polarisation transfer from the CT to the neighbouring |−3/2>→|−1/2> and |+1/2>→|+3/2> transitions during the frequency swept WURST pulse (Figure 3). *Spidyan* simulations further corroborated previous results demonstrating a loss in polarisation enhancement upon a larger strain in the ZFS distribution,[28] most likely as a result of first-order broadening of these transitions (Figure S.2.1). Further to this, larger D values also resulted in decreased polarisation, limiting the efficiency of polarisation transfer from the CT to higher spin transitions for complexes with D > 1 GHz (Figure S.2.2).

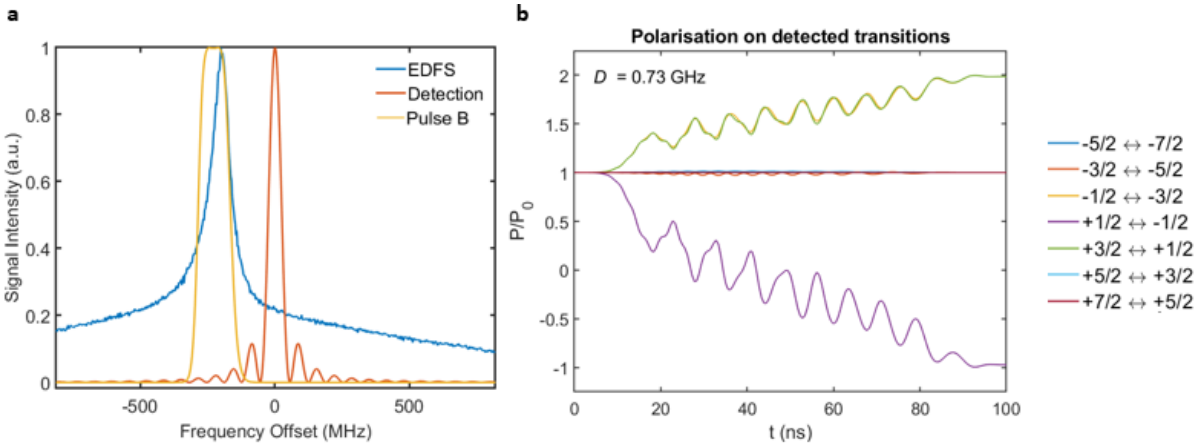

Figure 3: *a) Overlay of Hahn EDFS (blue) in the absence of a polarisation pulse of complex (**1**) and excitation profiles of the detection (rectangular, 16 ns) π-pulse (orange) and polarisation pulse, (pulse B, yellow) plotted as a function of the offset from the detection frequency (33.93 GHz). b) Spidyan simulations showing the polarisation on each EPR transition of complex (**1**) during the evolution of the polarising pulse (pulse B), noting similar levels of polarisation for both the |−3/2>→|−1/2> and |+1/2>→|+3/2> transitions,*

calculated for Q = 5, where Q is the critical adiabaticity value of the shaped pulse defined at its minimum as Q_{min} (Equation (1)).

A slight diminution of the enhancement on the |−3/2>→|−1/2> transition was observed if the polarisation pulses are not correctly tuned to the B_1 and bandwidth of the resonator cavity at the given frequency. This was most likely the result of oversaturation between spin manifolds by the shaped pulses, resulting in $|\Delta m_S| \geq 2$ transitions. Such transitions have previously been directly observed in a DEER experiment, measuring a bis-Gd(III) system, for chirp pump pulses with high adiabaticity factors.[35] These $|\Delta m_S| \geq 2$ transitions cause an effective overturning of the spin manifold into its neighbouring transition, thereby reducing the echo intensity at the EPR transition of interest. Therefore, we found for the Q-band measurements that it was imperative to measure and include the appropriate transfer function in the generation and application of the shaped polarisation pulse and it was also necessary to measure an amplitude sweep of the pulse as a function of echo intensity in order to achieve the highest sensitivity enhancement (Figure S.3.7).

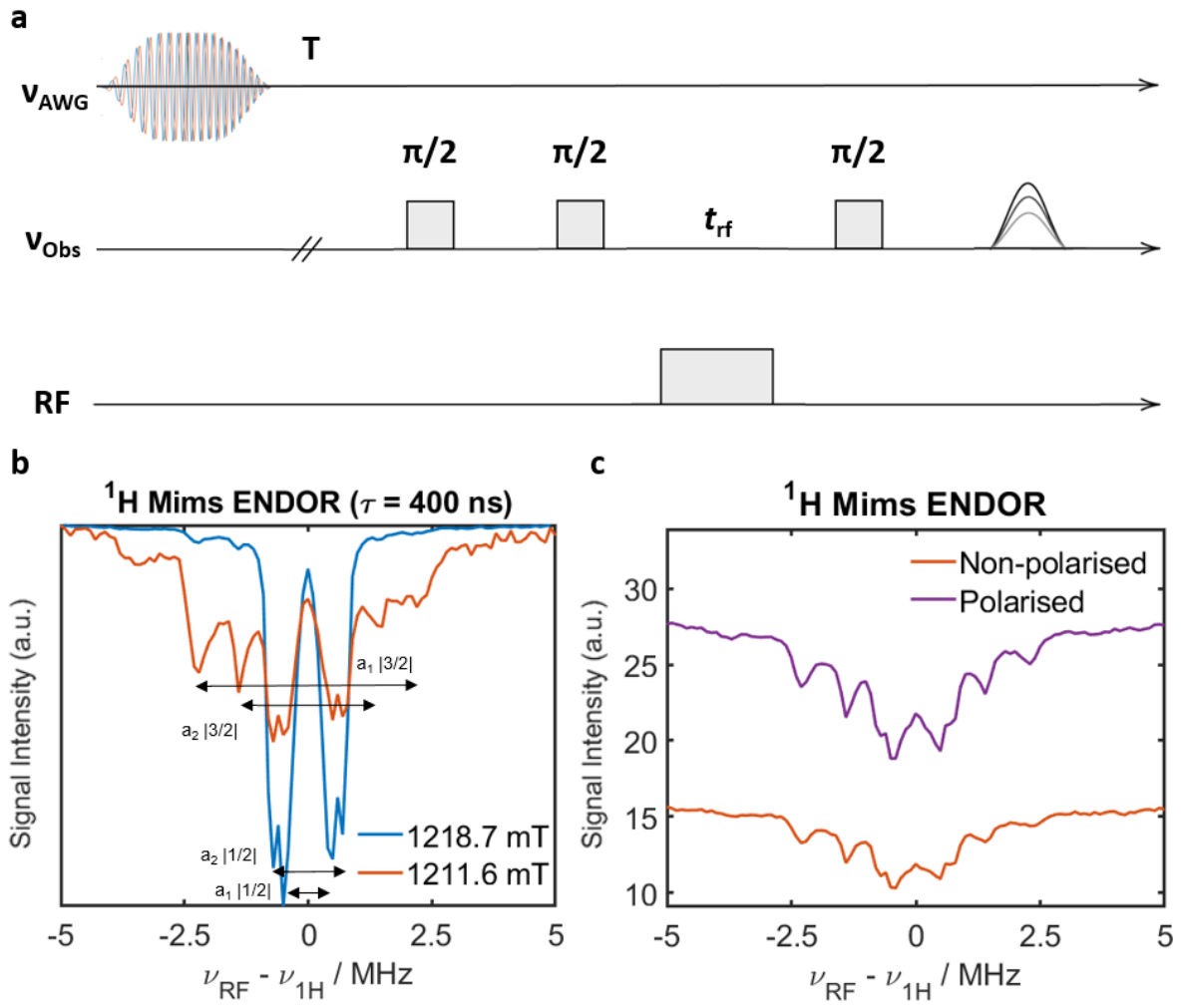

Figure 4: *a) Polarised Mims ENDOR pulse sequence. b) Non-polarised ^{1}H Mims ENDOR spectra of complex (**1**) at the CT, 1218.7 mT (blue), and targeting the transition whose largest component is the |─3/2>→|─1/2> manifold, 1211.6 mT (orange) with τ = 400 ns at 4.5 K, showing splitting of the different spin manifolds as described in the main text. c) Non-polarised (blue) and optimally polarised (purple) averaged ^{1}H Mims ENDOR spectra of complex (**1**) at a field position of 1211.6 mT (33.93 GHz), targeting the |─3/2>→|─1/2> transition, at 4.5 K.*

^{1}H Mims ENDOR detecting on the CT of (**1**) showed splitting due to two different protons with a_1 = 1 MHz and a_2 = 1.4 MHz (Figure 4b, blue), while the averaged ^{1}H Mims ENDOR spectrum (Figure 4c) targeting the |─3/2>→|─1/2> transition (individual plots with different τ values available in SI, Figure S.3.8) also showed contributions from the state with $|m_S|$ = 3/2. Pre-polarisation of the sequence with the tuned frequency swept shaped pulse (pulse B) gave an average enhancement factor of 1.82 at 1211.6 mT. Further, polarisation enhancements were consistent across a range of τ values (Figure S.3.9).

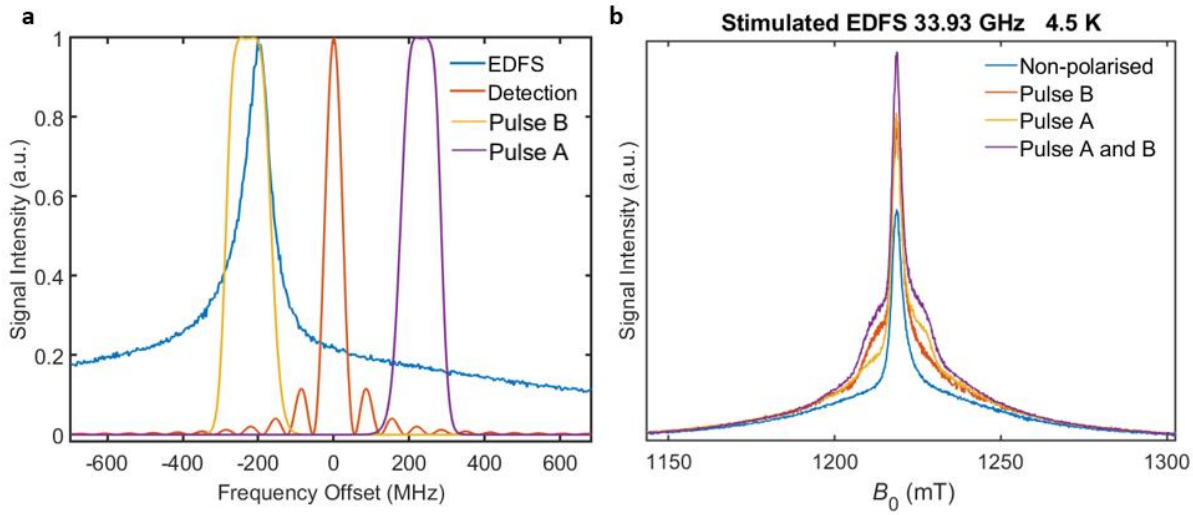

Figure 5: *a) Overlay of Hahn EDFS (blue) in the absence of a polarisation of (**1**) and excitation profiles of a detection π-pulse (rectangular, 16 ns, orange), for the stimulated echo sequence an 8 ns π/2 pulse was used, and polarisation pulses (pulse B - yellow, pulse A - purple) plotted as the offset from the detection frequency. b) Stimulated EDFS of complex (**1**) at 4.5 K (33.93 GHz) without polarisation (blue), polarisation with pulse B (orange), polarisation with pulse A (yellow), and polarisation with both pulse A and pulse B (purple).*

The best results were obtained upon the application of two pre-polarising frequency swept pulses (pulse B and pulse A), transferring polarisation from both the CT and part of the |─5/2>→|─3/2> and |─7/2>→|─5/2> transitions (Figure 5a). In a stimulated EDFS sequence

the largest enhancements were seen at the |−3/2>→|−1/2> transition for pulse B and |+1/2>→|+3/2> for pulse A, while the application of both pulse B and A gave the greatest enhancement factors of 2.3 and 2.1 at each respective field position (1211.6 mT and 1218.7 mT), compared to the non-polarised sequence (Figure 5b). The difference in enhancements between the two field positions is most likely due to the asymmetry in the CT and underlying transitions.

Spin dynamic simulations show that the total polarisation on the detected transition is higher than that seen in the experimental case (Figure 6b), most likely due to the fact that the frequency swept pulse (pulse A) is swept over a frequency range where the adiabatic condition may not be completely fulfilled for the length of the polarisation pulse used, even under bandwidth compensated conditions, resulting in a loss in the efficiency of polarisation transfer from the higher EPR transitions to the |−3/2>→|−1/2> transition. Spectrometers operating with non-resonant quasi-optical sample holders can provide instantaneous bandwidths of 1 GHz and may mitigate the reductions seen in polarisation transfer experiments by ensuring the adiabatic condition is met across the bandwidth of each tuned frequency swept polarisation pulse to give optimal sensitivity enhancement.[36] Further to this, it is noted that experimentally pulse A sweeps across a portion of both the |−5/2>→|−3/2> and |−7/2>→|−5/2> transitions, however from simulations it is suggested that most polarisation upon the application of pulse A is transferred from the |−5/2>→|−3/2> transition to both its neighbours. The experimental set-up and faster relaxation time of higher spin transitions coupled with the short T_m of complex (**1**) means that any polarisation of the |−7/2>→|−5/2> transition is not captured in the current experimental spectra. In polarised ^{1}H Mims ENDOR experiments, enhancement of the signal was found to be over 2.3 at 1211.6 mT (Figure 6c). Using a non-stochastic linear RF sweep resulted in an increase in echo intensity in the case of the polarised spectrum without detrimental heating effects at the sample. While the echo intensity is enhanced, the ENDOR efficiency remains constant between non-polarised and polarised spectra as this is not dependent on the sensitivity of the experiment. Some orientation selectivity may be expected as the polarising pulse A only inverts a sub-section of spins from the higher spin transitions, however due to the large distributions in ZFS parameters this is not seen for the studied complex in frozen solution. However, this will probably be an important consideration for polarisation transfer in complexes with very anisotropic hyperfine couplings and small distributions in ZFS parameters. In the studied complex these effects are further abolished,

most likely due to the symmetrical nature, and hence reduced orientations, of the proton hyperfine interaction (Figure S.3.10).

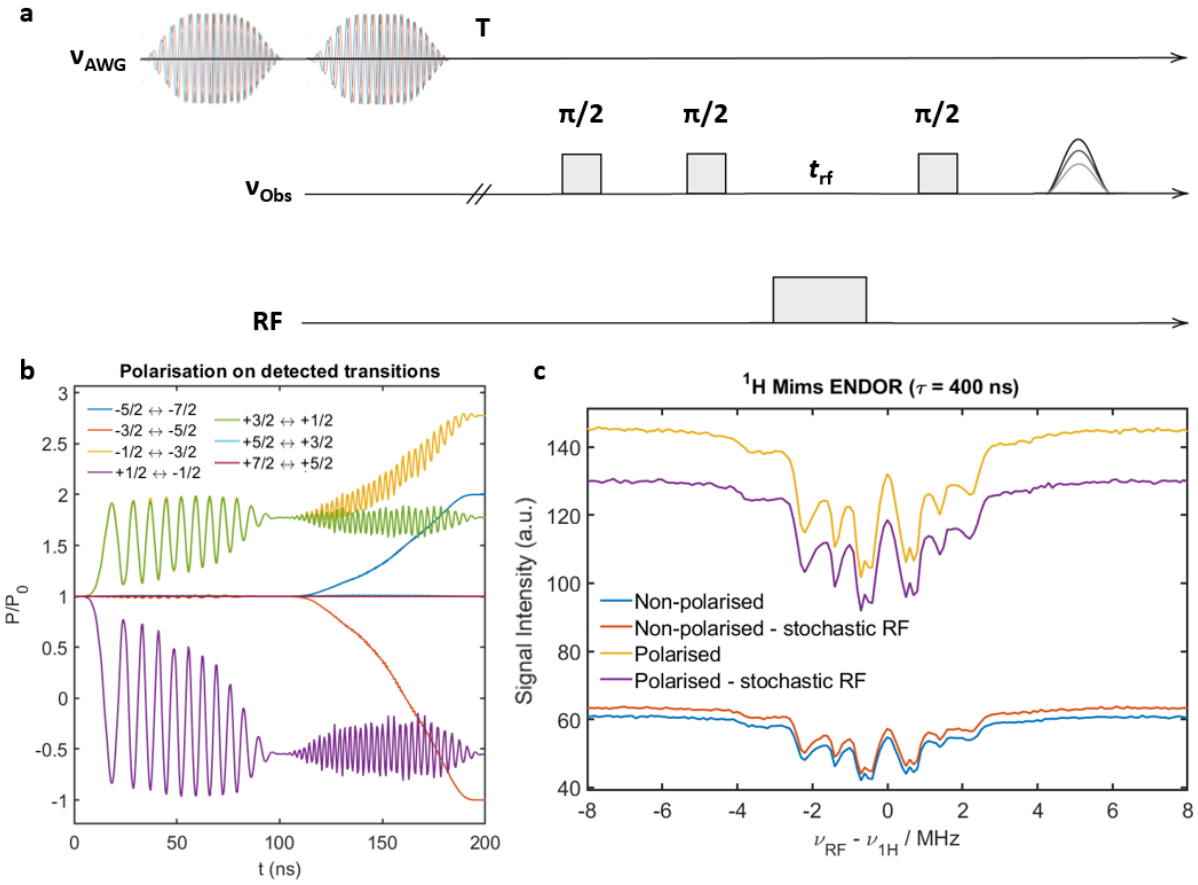

Figure 6: *a) Polarised Mims ENDOR sequence with two polarising pulses. b) Spidyan simulations showing the polarisation on the spin transitions of complex (**1**) during the evolution of the polarising pulses (pulse B and A) c) Non-polarised non-stochastic RF pulse (blue), stochastic RF pulse (orange), polarised non-stochastic RF pulse (yellow) and stochastic RF pulse (purple) ^{1}H Mims ENDOR spectra of complex (**1**) at a field position of 1211.6 mT (33.93 GHz) at 4.5 K, with τ = 400 ns.*

<u>W-band</u>

At W-band, polarisation transfer was investigated at 11.5 K using a Gd(III) BrPsPy-DO3A complex (**2**), which has been used previously to spin label proteins *via* native or engineered cysteines.[30] The complex has a ZFS constant of D = 1150 MHz which is ca. 60% larger than that of complex (**1**) used for Q-band measurements. The width of the higher spin transitions is therefore ca. 60% larger in (**2**), while the CT of both complexes have a similar width. The spin polarisation of the CT in W-band at 11.5K ($n_{-1/2}$-$n_{+1/2}$ ≈ 0.034) is comparable with that in Q-band at 4.5 K ($n_{-1/2}$-$n_{+1/2}$ ≈ 0.033).[37] At W-band, the length of the polarisation pulses used

were optimised to be 2 µs for efficient spin inversion, significantly longer than that used at Q-band due to the lower power available. Further, compensation of the pre-polarisation pulse shape for the cavity profile was not implemented at W-band. Under these conditions the value of variation in B_1, measured for a spin-1/2 system, across the pulse frequency profile (Figure S.3.3) caused a variation in Q_{min} from ca. 0.06 on the far side of the polarisation pulse to ca. 0.6 in the vicinity of the observer frequency, while these values fall below the ideal value of 5 for a spin-1/2 system, the high spin nature of Gd(III) reduces the required Q_{min}.[28] The parameters used for Hahn EDFS spectra recorded with two polarisation pulses preceding the sequence resulted in an enhancement factor of ca. 2.2 in spin echo intensity detecting on the |−3/2>→|−1/2> transition compared to the Hahn EDFS measured without polarisation pulses (Figure 7a). A similar enhancement factor at this detection frequency was observed using a stimulated EDFS sequence with time delays mirroring the Mims ENDOR sequence (Figure 7b). Parameters for the frequency swept WURST amplitude polarisation pulses used at W-band are given in Table S.3.3.

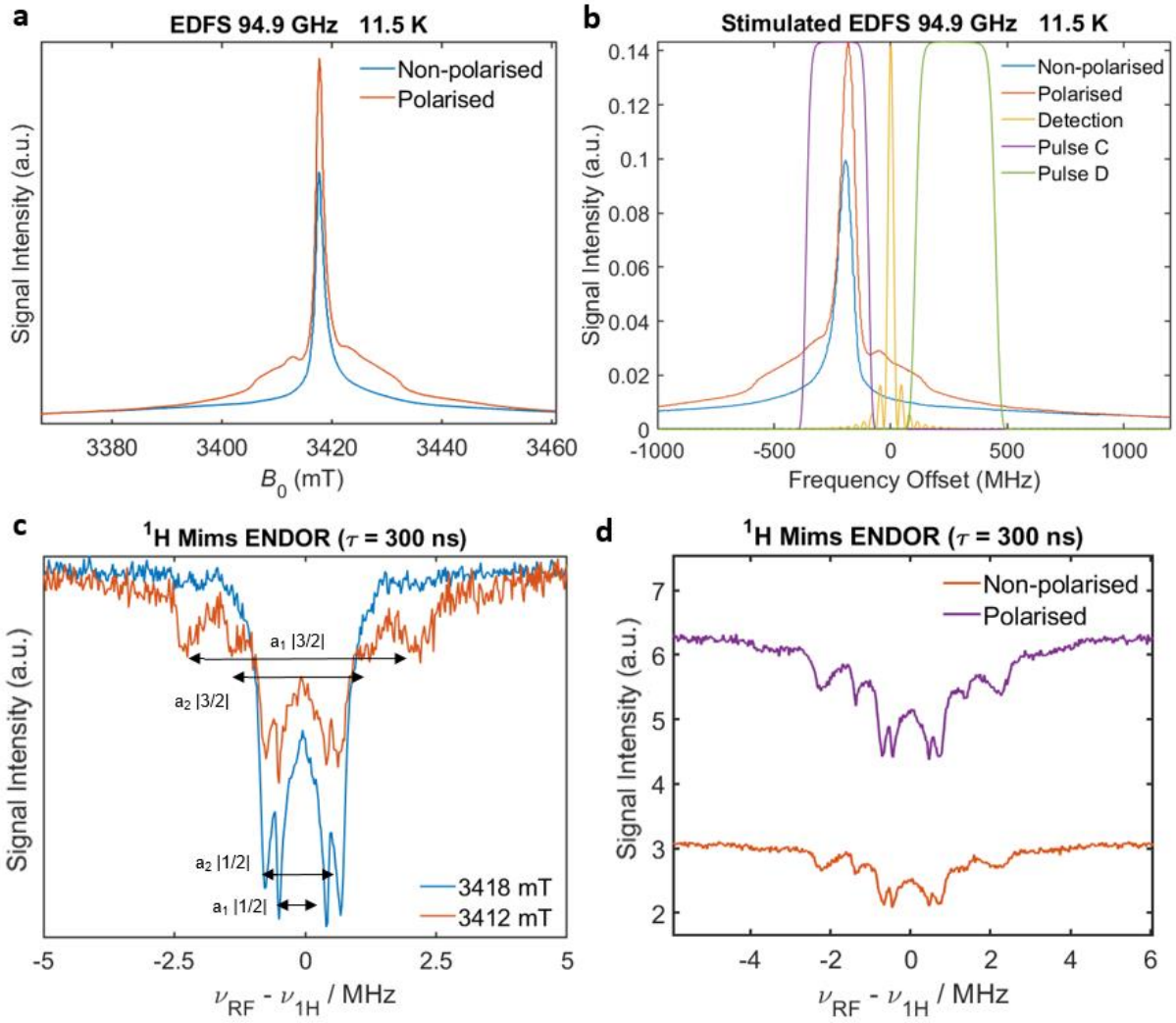

Figure 7: *a) Experimental non-polarised (blue) and polarised (orange) Hahn EDFS of (**2**). b) Experimental non-polarised (blue) and polarised (orange) stimulated EDFS of (**2**), showing the excitation profiles of a detection π-pulse (3412 mT, rectangular, 30 ns, yellow), for the stimulated echo sequence a 15 ns π/2 pulse was used, and of the pre-polarisation pulses (pulse C - purple, pulse D - green) as the frequency offset from the detection position. c) Non-polarised ^{1}H Mims ENDOR spectra of complex (**2**) at the CT, 3418 mT (blue) and targeting the |─3/2>→|─1/2> transition at 3412 mT (orange) with τ =300 ns at 11.5 K. d) Non-polarised (blue) and polarised (purple) ^{1}H Mims ENDOR spectra of complex (**2**) recorded at 3412 mT at 11.5 K.*

The ^{1}H Mims ENDOR spectra of (**2**) CT showed resolved splitting for 2 types of protons with a_1 = 0.9 MHz and a_2 = 1.45 MHz (Figure 7c, orange), consistent with the ENDOR spectra obtained at Q-band. ^{1}H ENDOR spectra of similar Gd(III) tags at W-band have previously been reported.[38] In the ENDOR spectra recorded outside the CT the same pair of doublets are observed, and in addition the signals with splitting $3a_1$ and $3a_2$ appear, which correspond to the contribution from the state with $|m_S|$ = 3/2. Unexpectedly, recorded ENDOR spectra remain symmetric on both sides (Figure 7c), and the reason may be the spherical arrangement of the protons around the Gd(III).[39] For ^{1}H Mims ENDOR spectra preceded by two polarisation pulses (pulse C and pulse D) placed either side of the |─3/2>→|─1/2> detection transition, an enhancement factor of ca. 2 was observed (Figure 7d). Similar to Q-band measurements, the shape of the ENDOR spectrum was not affected by the use of polarisation pulses, the ENDOR efficiency remained the same, and the enhancement measured was consistent across a range of tau values (Figure S.3.11).

Conclusions

In conclusion, we have used frequency swept WURST amplitude pulses to pre-polarise ^{1}H Mims ENDOR spectra for signal enhancement of the |─3/2>→|─1/2> transition of two model Gd(III) complexes at Q- and W-band frequencies. It was found that transferring polarisation from both the CT and regions of the |─5/2>→|─3/2> and |─7/2>→|─5/2> transitions gave enhancement factors of the |─3/2>→|─1/2> transition over 2.3 at Q-band and ca. 2 at W-band. The increased sensitivity of the echo at this detection position following polarisation, alongside lower temperatures, should result in the ability for high SNR measurements in HIHS systems, where detection of higher EPR transitions away from the CT is desired, particularly in systems where the magnitude and strain in ZFS parameters are < 1

GHz. As higher temperatures are generally easier to achieve and maintain on standard EPR set-ups, polarisation transfer from the CT can be seen as a means to mimic the gain in the Boltzmann distribution of the lower lying levels by thermal polarisation at high fields and low temperatures. Future applications of pre-polarisation away from the CT might include DEER with pump and detection frequencies set to be resonant either side of the CT in order to minimise spectral diffusion related to flip-flop transitions.[40] Additionally it may be possible to push the resolution of Gd(III)-^{19}F ENDOR based distance measurements to smaller coupling values, while avoiding the extremely low temperatures normally needed for efficient thermal polarisation of the corresponding EPR transitions. For example, detecting on the $|-3/2\rangle \rightarrow |-1/2\rangle$ transition should give resolved splitting of poorly resolved long (< 1.5 nm) Gd(III)-^{19}F intramolecular distances, with a greater than two factor gain in the signal intensity by pre-polarising the sequence. Current work is underway to demonstrate this in both model systems and in proteins.

Acknowledgements

A.M.B is grateful to The Royal Society and EPSRC for a Dorothy Hodgkin Fellowship (DH160004), and the University of Manchester for a Dame Kathleen Ollerenshaw Fellowship. A.M.B. also thanks the Royal Society of Chemistry for a Community for Analytical and Measurement Science (CAMS) fellowship. A.M.B. and C.J.R. thank The Royal Society for the Enhancement Award (RGF\EA\180287) which funded the doctoral studentship for C.J.R. C.J.R is further grateful to the Turing Scheme for funding to undertake a placement at the Weizmann Institute of Science. M.E.T thanks the BBSRC Doctoral Training Partnership 2, BB/M011208/1 for funding. This work was funded by the National Science Foundation USA-Israel Science Foundation program through BSF 2021617 (to D.G.). This research was made possible in part by the historic generosity of the Harold Perlman Family (D.G.). D. G. holds the Erich Klieger Professorial Chair in Chemical Physics. The authors acknowledge the Centre for Advanced Electron Spin Resonance at Oxford University, funded by the UK EPSRC (EP/L011972/1) and the EPSRC funded National Research facility at the University of Manchester (EP/W014521/1, NS/A000055/1, EP/V035231/1 and EP/S033181/1), for use of facility access and support. We are grateful to Prof. Christiane Timmel and Dr William Myers for help with experiments. A CC BY or equivalent license is applied to the Author Accepted Manuscript arising from this submission.

Conflicts of interest

There are no conflicts to declare.

References

[1] G. Feher, Observation of Nuclear Magnetic Resonances via the Electron Spin Resonance Line, Phys. Rev. 103 (1956) 376. https://doi.org/10.1103/PhysRev.103.834.

[2] M. Drescher, G. Jeschke, EPR Spectroscopy Applications in Chemistry and Biology, Springer Science & Business Media, 321, 2012.

[3] S. Sottini, P. Gast, A. Blok, G.W. Canters, D. Cavazzini, G.L. Rossi, E.J.J. Groenen, A Proton ENDOR Study of Azurin, Appl. Magn. Reson. 37 (2010) 219–227. https://doi.org/10.1007/s00723-009-0048-9.

[4] Y. Pokern, B. Eltzner, S.F. Huckemann, C. Beeken, J. Stubbe, I. Tkach, M. Bennati, M. Hiller, Statistical analysis of ENDOR spectra, PNAS. 118 (2021) 1–11. https://doi.org/10.1073/pnas.2023615118.

[5] C.W.M. Kay, E. Schleicher, K. Hitomi, T. Todo, R. Bittl, S. Weber, Determination of the *g*-matrix orientation in flavin radicals by high-field/high-frequency electron-nuclear double resonance, Magn. Reson. Chem. 43 (2005) 96–102. https://doi.org/10.1002/MRC.1667.

[6] S. Van Doorslaer, E. Vinck, The strength of EPR and ENDOR techniques in revealing structure–function relationships in metalloproteins, Phys. Chem. Chem. Phys. 9 (2007) 4620–4638. https://doi.org/10.1039/B701568B.

[7] F. Moro, L. Turyanska, J. Wilman, H.E.L. Williams, A.J. Fielding, A. Patanè, Surface Sensing of Quantum Dots by Electron Spins, Nano Lett. 16 (2016) 6343–6348. https://doi.org/10.1021/ACS.NANOLETT.6B02727.

[8] P.G. Baranov, S.B. Orlinskii, C. de Mello Donegá, J. Schmidt, High-Frequency EPR and ENDOR Spectroscopy on Semiconductor Quantum Dots, Appl. Magn. Reson. 39 (2010) 151. https://doi.org/10.1007/S00723-010-0151-Y.

[9] D. Lukoyanov, Z.-Y. Yang, D.R. Dean, L.C. Seefeldt, B.M. Hoffman, Is Mo Involved in Hydride Binding by the Four-Electron Reduced (E4) Intermediate of the Nitrogenase MoFe Protein?, J. Am. Chem. Soc. 132, 8 (2010) 2526–2527. https://doi.org/10.1021/ja910613m.

[10] R.A. Kinney, C.T. Saouma, J.C. Peters, B.M. Hoffman, Modeling the Signatures of Hydrides in Metalloenzymes: ENDOR Analysis of a Di-iron Fe(μ-NH)(μ-H)Fe Core, J. Am. Chem. Soc. 134, 30 (2012) 12637–12647. https://doi.org/10.1021/ja303739g.

[11] S. Van Doorslaer, A. Schweiger, Continuous Wave and Pulse EPR and ENDOR Study of Oxygenated Cobalt(II) Heme Model Systems, J. Phys. Chem. B. 104 (2000) 2919–2927. https://doi.org/10.1021/JP993668C.

[12] V. Hoeke, L. Tociu, D.A. Case, L.C. Seefeldt, S. Raugei, B.M. Hoffman, High-Resolution ENDOR Spectroscopy Combined with Quantum Chemical Calculations Reveals the Structure of Nitrogenase Janus Intermediate E4 (4H), J. Am. Chem. Soc. 141, 30 (2019) 11984–11996. https://doi.org/10.1021/jacs.9b04474.

[13] A. Martorana, G. Bellapadrona, A. Feintuch, E. Di Gregorio, S. Aime, D. Goldfarb, Probing protein conformation in cells by EPR distance measurements using Gd^{3+} spin

labeling, J. Am. Chem. Soc. 136 (2014) 13458–13465. https://doi.org/10.1021/JA5079392.

[14] S. Kucher, C. Elsner, M. Safonova, S. Maffini, E. Bordignon, In-Cell Double Electron-Electron Resonance at Nanomolar Protein Concentrations, J. Phys. Chem. Lett. 12 (2021) 3679–3684. https://doi.org/10.1021/ACS.JPCLETT.1C00048.

[15] A. Giannoulis, Y. Ben-Ishay, D. Goldfarb, Characteristics of Gd(III) spin labels for the study of protein conformations, 1st ed., Elsevier Inc., 2021. https://doi.org/10.1016/bs.mie.2021.01.040.

[16] A. Shah, A. Roux, M. Starck, J.A. Mosely, M. Stevens, D.G. Norman, R.I. Hunter, H. El Mkami, G.M. Smith, D. Parker, J.E. Lovett, A Gadolinium Spin Label with Both a Narrow Central Transition and Short Tether for Use in Double Electron Electron Resonance Distance Measurements, Inorg. Chem. 58, 5 (2019) 3015–3025. https://doi.org/10.1021/acs.inorgchem.8b02892.

[17] E. H. Abdelkader, A. Feintuch, X. Yao, L. A. Adams, L. Aurelio, B. Graham, D. Goldfarb, G. Otting, Protein conformation by EPR spectroscopy using gadolinium tags clicked to genetically encoded p-azido-L-phenylalanine, Chem. Commun. 51 (2015) 15898–15901. https://doi.org/10.1039/c5cc07121f.

[18] M. Judd, E.H. Abdelkader, M. Qi, J.R. Harmer, T. Huber, A. Godt, A. Savitsky, G. Otting, N. Cox, Short-range ENDOR distance measurements between Gd(III) and trifluoromethyl labels in proteins, Phys. Chem. Chem. Phys. 24 (2022) 25214–25226. https://doi.org/10.1039/D2CP02889A.

[19] M. Seal, W. Zhu, A. Dalaloyan, A. Feintuch, A. Bogdanov, D.G. Frydman, X.-C. Su, A.M. Gronenborn, D. Goldfarb, Gd(III)-19F Distance Measurements of Proteins in Cells by Electron-Nuclear Double Resonance, Angew. Chem. Int. Ed. e202218780 (2023).

[20] X. Tan, M. Bernardo, H. Thomann, C. P. Scholes, ^{17}O hyperfine and quadrupole interactions for water ligands in frozen solutions of high spin Mn^{2+}, J. Chem. Phys. 102 (1995) 2675–2690. https://doi.org/10.1063/1.468644.

[21] P. Caravan, A. V. Astashkin, A.M. Raitsimring, The gadolinium(III)-water hydrogen distance in MRI contrast agents, Inorg. Chem. 42 (2003) 3972–3974. https://doi.org/10.1021/IC034414F.

[22] B. Epel, P. Manikandan, P.M.H. Kroneck, D. Goldfarb, High-Field ENDOR and the Sign of the Hyperfine Coupling, Appl. Magn. Reson. 21 (2001) 287–297.

[23] P. Manikandan, R. Carmieli, T. Shane, A.J. Kalb, D. Goldfarb, W-Band ENDOR investigation of the manganese-binding site of concanavalin A: Determination of proton hyperfine couplings and their signs, J. Am. Chem. Soc. 122, 14 (2000) 3488–3494. https://doi.org/10.1021/JA993395Z.

[24] A.M. Raitsimring, A. V. Astashkin, D. Baute, D. Goldfarb, P. Caravan, W-band ^{17}O pulsed electron nuclear double resonance study of gadolinium complexes with water, J. Phys. Chem. A. 108, 35 (2004) 7318–7323. https://doi.org/10.1021/JP040306I.

[25] P.E. Spindler, P. Schöps, A.M. Bowen, B. Endeward, T.F. Prisner, Shaped pulses in EPR, EMagRes. 5 (2016) 1477–1492. https://doi.org/10.1002/9780470034590.emrstm1520.

[26] D. Iuga, H. Schäfer, R. Verhagen, A.P.M. Kentgens, Population and Coherence Transfer Induced by Double Frequency Sweeps in Half-Integer Quadrupolar Spin Systems, J. Magn. Reson. 147 (2000) 192–209. https://doi.org/10.1006/JMRE.2000.2192.

[27] A.P.M. Kentgens, R. Verhagen, Advantages of double frequency sweeps in static, MAS and MQMAS NMR of spin I = 3/2 nuclei, Chem. Phys. Lett. 300 (1999) 435–443. https://doi.org/10.1016/S0009-2614(98)01402-X.

[28] A. Doll, M. Qi, S. Pribitzer, N. Wili, M. Yulikov, A. Godt, G. Jeschke, Sensitivity enhancement by population transfer in Gd(III) spin labels, Phys. Chem. Chem. Phys. 17 (2015) 7334–7344. https://doi.org/10.1039/c4cp05893c.

[29] I. Kaminker, A. Potapov, A. Feintuch, S. Vega, D. Goldfarb, Population transfer for signal enhancement in pulsed EPR experiments on half integer high spin systems, Phys. Chem. Chem. Phys. 11 (2009) 6799–6806. https://doi.org/10.1039/B906177K.

[30] Y. Yang, F. Yang, Y.J. Gong, T. Bahrenberg, A. Feintuch, X.-C. Su, D. Goldfarb, High Sensitivity In-Cell EPR Distance Measurements on Proteins using an Optimized Gd(III) Spin Label, J. Phys. Chem. Lett. 9 (2018) 6119–6123. https://doi.org/10.1021/acs.jpclett.8b02663.

[31] D. Goldfarb, Y. Lipkin, A. Potapov, Y. Gorodetsky, B. Epel, A.M. Raitsimring, M. Radoul, I. Kaminker, HYSCORE and DEER with an upgraded 95 GHz pulse EPR spectrometer, J. Magn. Reson. 194 (2008) 8–15. https://doi.org/10.1016/J.JMR.2008.05.019.

[32] S. Stoll, A. Schweiger, EasySpin, a comprehensive software package for spectral simulation and analysis in EPR, J. Magn. Reson. 178 (2006) 42–55. https://doi.org/10.1016/j.jmr.2005.08.013.

[33] S. Pribitzer, A. Doll, G. Jeschke, SPIDYAN, a MATLAB library for simulating pulse EPR experiments with arbitrary waveform excitation, J. Magn. Reson. 263 (2016) 45–54. https://doi.org/10.1016/J.JMR.2015.12.014.

[34] G. Jeschke, S. Pribitzer, A. Doll, Coherence Transfer by Passage Pulses in Electron Paramagnetic Resonance Spectroscopy, J. Phys Chem. B 119, 43 (2015) 13570–13582 https://doi.org/10.1021/ACS.JPCB.5B02964.

[35] A. Doll, M. Qi, N. Wili, S. Pribitzer, A. Godt, G. Jeschke, Gd(III)-Gd(III) distance measurements with chirp pump pulses, J. Magn. Reson. 259 (2015) 153–162. https://doi.org/10.1016/J.JMR.2015.08.010.

[36] P.A.S. Cruickshank, D.R. Bolton, D.A. Robertson, R.I. Hunter, R.J. Wylde, G.M. Smith, A kilowatt pulsed 94 GHz electron paramagnetic resonance spectrometer with high concentration sensitivity, high instantaneous bandwidth, and low dead time, Rev. Sci. Instrum. 80, 103102 (2009). https://doi.org/10.1063/1.3239402.

[37] D. Goldfarb, Metal-Based Spin Labeling for Distance Determination, in: Structural Information from Spin-Labels and Intrinsic Paramagnetic Centres in the Biosciences, 2013 pp. 163–204..

[38] A. Collauto, A. Feintuch, M. Qi, A. Godt, T. Meade, D. Goldfarb, Gd(III) complexes as paramagnetic tags: Evaluation of the spin delocalization over the nuclei of the ligand, J. Magn. Reson. 263 (2016) 156–163. https://doi.org/10.1016/J.JMR.2015.12.025.

[39] D. Baute, D. Goldfarb, The ^{17}O hyperfme interaction in $V^{17}O(H_2{}^{17}O)_6{}^{2+}$ and

$Mn(H_2{}^{17}O)_6{}^{2+}$ determined by high field ENDOR aided by DFT calculations, J. Phys. Chem. A. 109 (2005) 7865–7871. https://doi.org/10.1021/JP052132Q.

[40] H.E.L. Mkami, R.I. Hunter, P.A.S. Cruickshank, M.J. Taylor, J.E. Lovett, A. Feintuch, M. Qi, A. Godt, G.M. Smith, High-sensitivity Gd^{3+}-Gd^{3+} EPR distance measurements that eliminate artefacts seen at short distances, J. Magn. Reson. 1 (2020) 301–313. https://doi.org/10.5194/MR-1-301-2020.

TOC